Volume 99 · Number 8 · August 2012

114 Naturwissenschaften

Naturwissenschaften

THE SCIENCE OF NATURE

Volume 99 · Number 8 · August 2012 • pp xx

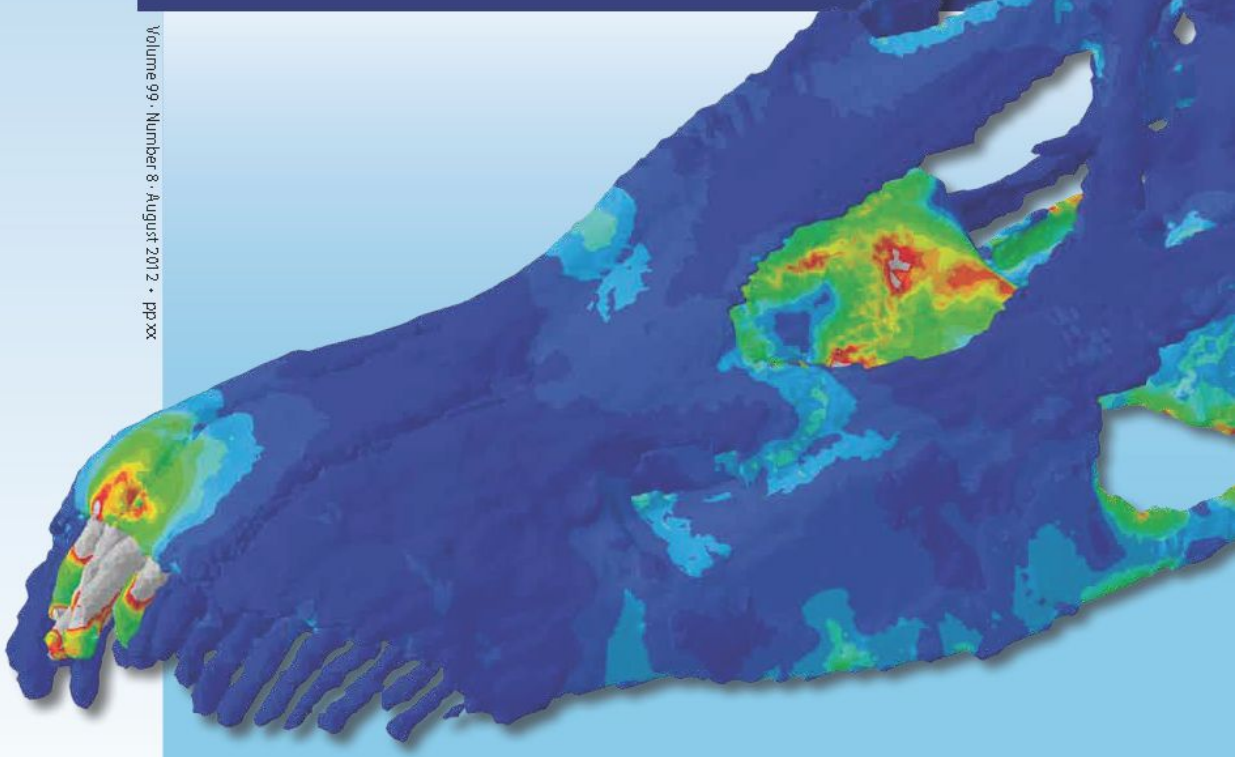

Organ der Gesellschaft Deutscher Naturforscher und Ärzte

Organ der Hermann von Helmholtz-Gemeinschaft Deutscher Forschungszentren

Springer

Naturwissenschaften (2012) 99:637–643
DOI 10.1007/s00114-012-0944-y

ORIGINAL PAPER

Cranial biomechanics of *Diplodocus* (Dinosauria, Sauropoda): testing hypotheses of feeding behaviour in an extinct megaherbivore

Mark T. Young · Emily J. Rayfield · Casey M. Holliday · Lawrence M. Witmer · David J. Button · Paul Upchurch · Paul M. Barrett

Received: 9 January 2012 / Revised: 26 June 2012 / Accepted: 28 June 2012 / Published online: 12 July 2012

Abstract Sauropod dinosaurs were the largest terrestrial herbivores and pushed at the limits of vertebrate biomechanics and physiology. Sauropods exhibit high craniodental diversity in ecosystems where numerous species co-existed, leading to the hypothesis that this biodiversity is linked to niche subdivision driven by ecological specialisation. Here, we quantitatively investigate feeding behaviour hypotheses for the iconic sauropod *Diplodocus*. Biomechanical modelling, using finite element analysis, was used to examine the performance of the *Diplodocus* skull. Three feeding behaviours were modelled: muscle-driven static biting, branch stripping and bark stripping. The skull was found to be 'over engineered' for static biting, overall experiencing low stress with only the dentition enduring high stress. When branch stripping, the skull, similarly, is under low stress, with little appreciable difference between those models. When simulated for bark stripping, the skull experiences far greater stresses, especially in the teeth and at the jaw joint. Therefore, we refute the bark-stripping hypothesis, while the hypotheses of branch stripping and/or precision biting are both consistent with our findings, showing that branch stripping is a biomechanically plausible feeding behaviour for diplodocids. Interestingly, in all simulations, peak stress is observed in the premaxillary–maxillary 'lateral plates', supporting the hypothesis that these structures evolved to dissipate stress induced while feeding. These results lead us to conclude that the aberrant craniodental form of *Diplodocus* was adapted for food procurement rather than resisting high bite forces.

Keywords Finite element analysis · Palaeobiology · Herbivory · Sauropod dinosaur

Communicated by: Robert Reisz

Electronic supplementary material The online version of this article (doi:10.1007/s00114-012-0944-y) contains supplementary material, which is available to authorized users.

M. T. Young · E. J. Rayfield · D. J. Button
School of Earth Sciences, University of Bristol,
Bristol BS8 1RJ, UK

M. T. Young · P. M. Barrett (✉)
Department of Palaeontology, The Natural History Museum,
London SW7 5BD, UK
e-mail: P.Barrett@nhm.ac.uk

C. M. Holliday
Department of Pathology and Anatomical Sciences,
University of Missouri,
Columbia, MO 65212, USA

L. M. Witmer
Department of Biomedical Sciences, Ohio University,
Athens, OH 45701, USA

P. Upchurch
Department of Earth Sciences, University College London,
London WC1E 6BT, UK

Present Address:
M. T. Young
School of Geosciences, University of Edinburgh,
Crew Building, The King's Buildings,
West Mains Road,
Edinburgh EH9 3JW, UK

Present Address:
M. T. Young
Institute of Biodiversity,
Animal Health and Comparative Medicine, University of Glasgow,
University Avenue,
Glasgow G12 8QQ, UK

Introduction

Sauropod dinosaurs were the largest terrestrial tetrapods in Earth's history. Throughout the Jurassic and Cretaceous, their size continued to increase, reaching maximum estimated body masses of 70 tonnes or more (Upchurch et al. 2004). Remarkably, in the Late Jurassic numerous species of these multi-tonne herbivores exhibited high degrees of sympatry, as shown by the sauropod faunas preserved in the Morrison Formation of western North America, the Tendaguru Beds of Tanzania and the Upper Shaximiao Formation of China (Upchurch and Barrett 2000; Mannion et al. 2011). Recent studies have suggested that niche partitioning, maintained via morphological differentiation, enabled this high biodiversity (Upchurch and Barrett 2000; Whitlock 2011). In the Morrison Formation and elsewhere, this differentiation relates to craniodental morphology and function, as well as to differences in postcranial anatomy, such as fore to hindlimb length ratios and neck function. The Morrison sauropod fauna includes at least eight genera potentially containing around 18 species: *Amphicoelias*, *Apatosaurus*, *Barosaurus*, *Brachiosaurus*, *Camarasaurus*, *Diplodocus*, *Haplocanthosaurus* and *Suuwaasea* (Mannion et al. 2011). Among these, diplodocoids, best characterised by *Diplodocus* itself, have extremely unusual craniodental morphologies. Among other features, the rostrum is elongate with the external nares strongly retracted posterodorsally to lie above the orbits; the tooth row is restricted to the anterior-most margin of the upper and lower jaws; the tooth crowns are apicobasally elongate with slight-to-moderate labiolingual compression and oblique wear facets on the labial surface (see the electronic supplementary material, Fig. S1), and the articular fossa was rostrocaudally elongate and shallow (a morphology often associated with translational mandibular movement or propaliny) (Holland 1906; Barrett and Upchurch 1994; Calvo 1994; Wilson and Sereno 1998; Upchurch and Barrett 2000). The overall craniodental morphology and tooth macro- and microwear have generated numerous conflicting hypotheses of feeding behaviour for *Diplodocus*. For example, it has been suggested that the teeth of *Diplodocus* were simply used during standard vertical occlusion for the slicing of vegetation (Calvo 1994). Other authors have argued that the procumbent teeth were incapable of occlusion (Barrett and Upchurch 1994). This, coupled with unusual patterns of tooth wear, in which both upper and lower tooth wear facets face labially (electronic supplementary material, Fig. S1B), gave rise to a unique 'branch stripping' model of feeding, with *Diplodocus* raking or combing its teeth through plant matter to pull leaves and shoots from branches using either the mandible or upper jaw independently (unilateral branch stripping; Barrett and Upchurch 1994) or using upper and lower jaws concurrently (bilateral branch stripping; Barrett and Upchurch 1994; Coombs 1975). Other suggestions have included precision plucking (associated with molluscivory; e.g. Sternfeld in Holland 1910), raking seaweed from rocks (Holland 1906), piscivory (Tornier 1911) and bark stripping (Holland 1924; Bakker 1986). More recently, Whitlock (2011) examined dental microwear patterns across numerous diplodocoid species and concluded that branch stripping was less plausible than other hypothesised feeding behaviours. Understanding the function and ecology of extinct organisms poses particular challenges, especially in the case of sauropods where no direct extant analogue exists.

One way to quantify, compare and better understand the function and mechanical behaviour of unusual morphologies is through biomechanical modelling. One such technique is finite element analysis (FEA), a computational method that reconstructs stress and strain within a structure after the application of performance-related loads. Finite element analysis has been used with increasing frequency in palaeontology and zoology to assess biomechanical performance (e.g. Dumont et al. 2005; Richmond et al. 2005; Rayfield 2007). Results of an FEA reveal 'hot spots' of functional stress, strain or deformation, the intensity of which can then be related to morphological features and the loading environment. This offers a means to test the biomechanical consequences of unusual or extreme morphologies. In the simplest sense, making bones thinner or thicker can increase or decrease stresses accordingly, and changing the load magnitudes and loading profile will modify the mechanical behaviour of the structure. It follows, therefore, that the different feeding regimes postulated for *Diplodocus* will generate different signature mechanical behaviours in the skull. 'Finite element structure synthesis' has previously been applied to principles of sauropod skull architecture (Witzel et al. 2011), but finite element methods have not been used to provide rigorous tests of sauropod feeding hypotheses thus far.

We used FEA to subject the skull of *Diplodocus* to simulated feeding loads for three hypothesised feeding behaviours: muscle-driven static biting (occlusion), unilateral branch stripping and bark stripping. The aim of our analysis is to test how occlusion and branch stripping comparatively influence skull biomechanics. We then test how behaviours, such as bark stripping, further compromise skull behaviour. Although bark stripping has received little support in the literature, testing of this hypothesis was deemed appropriate in order to elucidate how the *Diplodocus* skull would have responded to a range of feeding-induced mechanical forces. Finally, we comment on the relative likelihood of each postulated feeding scenario.

Materials and methods

A three-dimensional model of a complete *Diplodocus longus* skull (Carnegie Museum (CM) of Natural History, Pittsburgh, PA, CM 11161; electronic supplementary material, Fig. S1) was created using computed tomographic scanning. The skull

was scanned at the O'Bleness Memorial Hospital (Athens, OH, USA), producing 290 coronal slices, with 512 transaxial slices in both perpendicular planes, separated by 0.2-mm intervals. The fossil bone was digitally extracted from the surrounding rock matrix using the three-dimensional imaging software AMIRA (v. 4.1.2, Mercury Computing Systems, USA; electronic supplementary material, Fig. S2A). It was necessary to digitally correct some bones in AMIRA due to breakage, distortion and other imperfections of the fossil (Electronic supplementary material for further details). The 3D model was compared to cranial material held in the Carnegie Museum and the National Museum of Natural History (Washington, D.C.) to aid reconstruction and to improve accuracy. Segmented slice data from the AMIRA 3D model was imported into SCANIP v. 2.1 Build 149 (Simpleware Ltd, UK) to produce a smoothed skull surface model. In SCANFE v. 2.0 (Simpleware Ltd, UK) the three-dimensional surface model was meshed, creating a solid geometry consisting of approximately 91 % tetrahedral and 9 % hexahedral elements. The final mesh had 906,257 elements (electronic supplementary material, Fig. S2B).

Material properties and boundary conditions were assigned to the mesh using the finite element (FE) software ABAQUS (v. 6.7, Simulia, USA). The exact material properties, constraints and loading regime in extinct taxa cannot be modelled with complete accuracy (Richmond et al. 2005), and FE studies on extinct taxa are also hindered by the inability to directly measure material properties from fossil bone (Rayfield 2007). Nevertheless, as adult Late Jurassic neosauropod skeletons (such as that of *Diplodocus*) are characterised by Haversian bone (Curry 1999), material properties of extant histological analogues were used as a proxy. Three tissue types were modelled: cranial bone, dentine and enamel, all of which were treated as homogenous and isotropic materials to avoid introducing additional assumptions (see the Electronic supplementary material for further details). Both the constraints and loading regimes must be as biologically realistic as possible to ensure feeding biomechanical performance is adequately tested. To model standard occlusion, the apical surfaces of the premaxillary tooth crowns were constrained from moving dorsoventrally using a distributing coupling constraint (DCC) in ABAQUS v. 6.7. The DCC evenly distributes the boundary constraint across the apical surfaces of the teeth, but rather than directly fixing nodes; it uses a series of rigid links to connect the teeth to a constraint control point located 'in space', ventral to the apex surfaces (see the electronic supplementary material, Fig. S3). This type of constraint minimises artificially high stresses generated at the teeth when this region is directly constrained from movement, thus producing a more realistic distribution of cranial stress. We present here data from models constrained at four premaxillary teeth (two left and two right), thereby simulating biting a piece of vegetation roughly equivalent in size to a small tree branch. Sensitivity analyses constraining either 8 or 14 teeth that are intended to model bites on larger objects are explained in the Supplementary information. The mandibular condyles of both quadrates were constrained using a DCC, preventing transverse and translational motion (see the electronic supplementary material for condylar reaction forces and Fig. S3A). The loading regime in the FE model simulation replicated the contraction of six jaw-closing muscles (musculus (M.) adductor mandibulae externus superficialis, M. adductor mandibulae externus profundus, M. adductor mandibulae posterior, M. pterygoideus dorsalis, M. pterygoideus ventralis and M. pseudotemporalis superficialis) (see the electronic supplementary material, Fig. S6).

The method used to create the jaw-closing muscle reconstructions has previously been outlined (Holliday 2009) and is explained further in the Electronic supplementary material. In order to visually compare the FE models, von Mises stresses were plotted, as they indicate regional deformation as a function of the three principal stresses, and are good predictors of failure under ductile fracture (Dumont et al. 2005), which elastic materials, such as bone, undergo (Nalla et al. 2003). In order to model the branch- and bark-stripping feeding regimes, an additional force was applied directly to the apices of the premaxillary teeth. For the branch-stripping model, the additional force was estimated from the shear strength of plant parenchyma, 1 MN m^{-2} (Niklas 1992; K. J. Niklas, pers. comm.). The area of tooth-food contact was calculated for a single tooth by measuring the surface area of the apical surface of the tooth. This area was then multiplied by the number of teeth considered to contact the plant matter (4, 8 and 14 teeth, see above). Forces required to shear parenchyma (Niklas 1992) were calculated as: area of tooth apical surface (s) in contact with plant matter (m^2)×shear stress. For the 'four-tooth' contact model, this equated to a force of 100 N (for other tooth contact models, see calculations in the electronic supplementary material, Table S2). This branch-stripping force was directed anteriorly (i.e. parallel to the long axis of the skull; see Electronic supplementary information). This was to simulate resistance of the parenchyma as the animal retracted its head to detach plant matter. For the bark-stripping model, the additional force was estimated from the shear strength of linden wood (a wood of intermediate strength (see Niklas 1992; 730 N for four-tooth contact). This force was directed along the apicobasal axis of the loaded teeth (see Electronic supplementary information).

Due to uncertainties in the exact mechanical properties of the *Diplodocus* skull and associated soft tissues, we do not rely on the absolute values of the von Mises stresses generated by the analyses, as these are likely to differ somewhat from measurements that could have only been obtained in vivo. Instead, we use relative differences in the extent and magnitude of the stresses identified when comparing the results from our models—such differences still allow major functional trends to be identified with confidence.

Results

Visual inspection of the contour plot for the *Diplodocus* static-biting FE model shows that the rostrum, braincase and skull roof experienced low stresses during a muscle-driven bite (Fig. 1a; electronic supplementary material, Fig. S7). Five regions possess peaks of functionally induced stress: (1) the dorsal surface of the pterygoids, (2) midway along the palatine midline, (3) rostral corner of the postorbital-squamosal suture, (4) mediocaudal face of the quadrates and (5) the rostral margin of the palatine (Fig. 1a; electronic supplementary material, Fig. S7). Moderate levels of stress are observed along the dorsal and ventral margins of the pterygoid, the dorsal margin of the quadratojugal, along the lateral edge of the squamosal, the posterior surface of the quadrate and the dorsal and ventral surfaces of the palatine (Fig. 1a; electronic supplementary material, Fig. S7). In addition, moderately low levels of stress accumulate in the distal half of the basipterygoid process and the lateral surfaces of the squamosal (Fig. 1a; electronic supplementary material, Fig. S7).

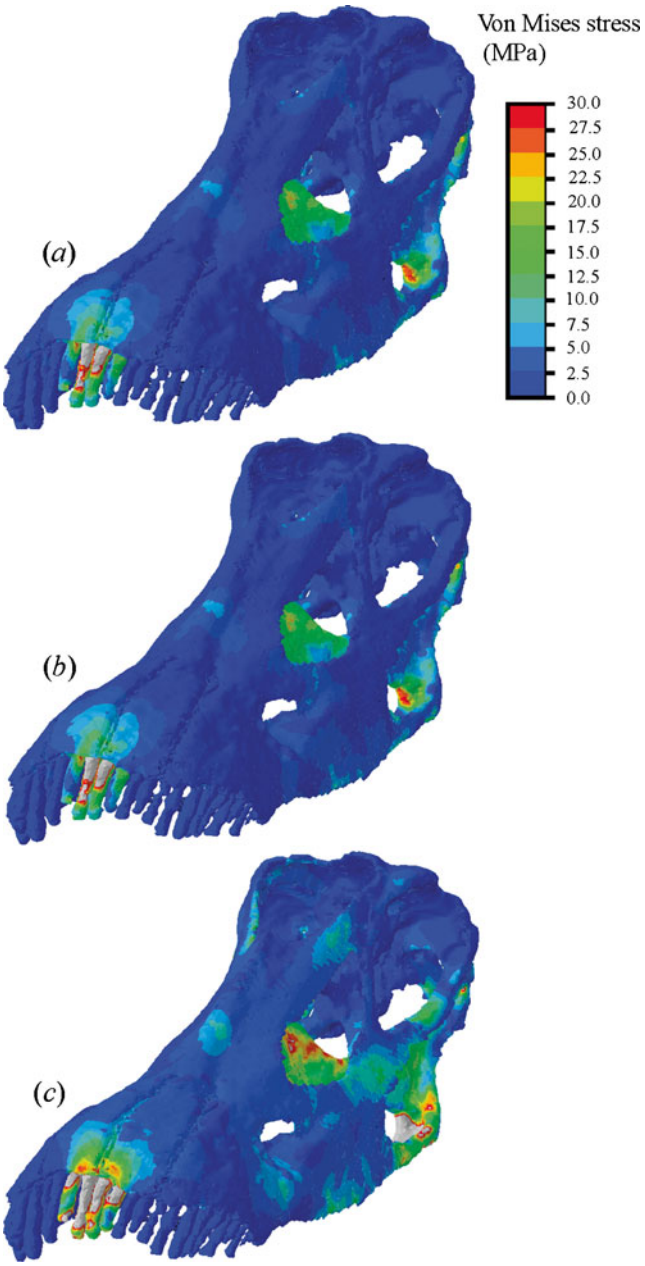

Fig. 1 *D. longus* skull von Mises stress contour plots in oblique view, four premaxillary teeth loaded for: (**a**) static biting, (**b**) branch stripping and (**c**) bark stripping

The regions with the thickest bone, the dentigerous portion of the maxilla and the bones forming the braincase and skull roof experience very low levels of stress, although the dentigerous portion of the premaxilla exhibits higher stress. Stresses at the synovial basipterygopterygoid and quadratosquamosal joints are low (Fig. 1a; electronic supplementary material, Fig. S7). The low stress at these joints and the hypothesised reduction of the M. protractor pterygoideus are congruent with the interpretation that the *Diplodocus* skull was akinetic (Upchurch and Barrett 2000; Holliday and Witmer 2008). The teeth experience high stresses, yet these may be artificially inflated in this region by excluding the periodontal ligament from our model (Toms and Eberhardt 2003; Cattaneo et al. 2005; Gröning et al. 2011; Panagiotopoulou et al. 2011) and the proximity to the constraint fixing the teeth. Further regions of moderate stress, which may also be artificially inflated (because of their proximity to the fixed jaw joint), are the proximoventral surface of the basipterygoid processes and along the dorsal edge of the left quadratojugal-quadrate suture (Fig. 1a; electronic supplementary material, Fig. S7). The overall patterns of von Mises stress in the static biting and branch-stripping models are very similar (Fig. 1a, b; electronic supplementary material, Figs. S7 and S8). Minor differences in the magnitudes of the stresses in these models result from the additional load that was applied to the branch-stripping model in order to represent the force needed to detach leaves/stems from the parent plant.

By contrast, the bark-stripping model (Fig. 1c, electronic supplementary material, Fig. S9) has the same regions of peak high stress as the other feeding regimes, and yet, stresses are of a far higher magnitude. Generalised low stress is more extensive across the skull in the bark-stripping model, and large regions of moderate stress are present in the thinnest bones of the skull. Moderate levels of stress occur at: the palatal surface of the maxilla, especially around the maxillary-ectopterygoid suture; the lateral surface of the maxilla (especially along the ventral margin) and the lateral surface of the quadratojugal. There are localised peaks of high stress present along both the dorsal and ventral margins of the quadratojugal (Fig. 1c; electronic supplementary material, Fig. S9). A notable increase in stress magnitude in the bark-

stripping model occurs at the dentigerous region of the premaxilla and palatal surface of the premaxilla and maxilla adjacent to the teeth. A region of low von Mises stress along the lateral margin of the maxillae is also more extensive in the bark-stripping model than in the other two models (Fig. S10). Comparisons between all three feeding models for bites, involving 4, 8 or 14 teeth, are provided in Fig. S10.

Mean nodal stress values from 16 different regions of the skull support the contention that, of the three feeding models, the bark-stripping model experiences the greatest stress (see Fig. 2 and electronic supplementary material, Table S4 for further details). There is very little difference in the mean nodal stress values at these loci between the static-biting and branch-stripping models.

Discussion

The skull of *Diplodocus* was generally subjected to low stress when muscle-only contractile forces are modelled. Although we cannot state that our modelled stresses are generated by the exact loads that the skull experienced during life, the adductor muscle reconstructions are as accurate as currently possible, and the resulting loads are low enough in magnitude that the skull appears not to be compromised by muscle-driven biting, consistent with the 'horizontal slicing' hypothesis (Calvo 1994). Indeed, it would be unexpected and indicative of error in our models if the skull could not withstand the load generated by its own adductor muscles. These results are even more interesting when we consider that

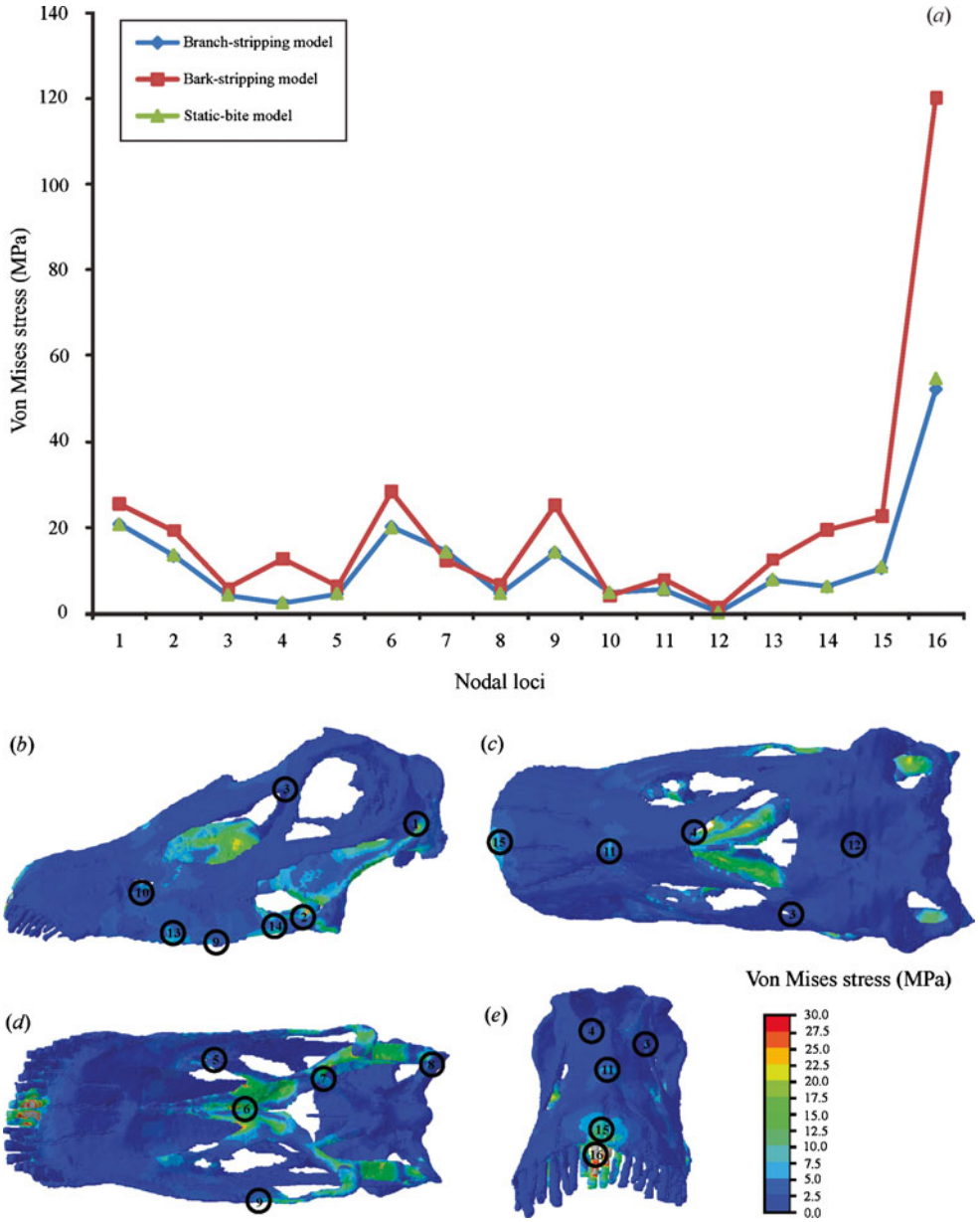

Fig. 2 Graph of mean von Mises stress from the three *D. longus* feeding models (**a**). The locations of the 16 nodal loci are shown in parts (**b**–**e**) (labels are on the static-biting model). These 16 locations were chosen as they cover a large part of the skull, including regions of peak functionally induced stress and regions of low stress, thereby ensuring a fair comparison of the potential differences in stress distribution between the feeding models. Where possible, we chose sutural junctions. The mean values were calculated by taking the mean of ten adjacent nodes at each locus. The exact locations are in the electronic supplementary material, Table S4

100 % muscle contraction and the highest specific tension of adductor muscles are assumed. These assumptions likely overestimate the muscle contractile forces. Our results are also fully consistent with the hypothesis that *Diplodocus* could branch strip (Coombs 1975; Barrett and Upchurch 1994), given the low levels of stress that are observed in these feeding models. On the basis of these results, it is plausible that *Diplodocus* was capable of using both standard vertical biting and branch stripping to harvest foliage (Christiansen 2000). However, the absence of a precise occlusion (Barrett and Upchurch 1994; contra Calvo 1994) suggests that under either of these scenarios, the teeth were primarily used to grip (rather than shear through) vegetation, which would then be detached from the parent plant by retraction or rotation of the head relative to the parent plant. In both models, the skull is not 'overloaded', as even with very high muscle tension of 392 kPa stresses in the skull do not, by some margin, exceed what is physiologically unsafe for bone.

The bark-stripping model produced a very different magnitude of stress. In the thinnest bones of the skull, moderate to very high peaks of stress were observed. In conjunction with the remarkably high stresses that the teeth endured, it is unlikely that the dentition or teeth-bearing bones of the skull could have withstood the forces involved in stripping bark from trees. Consequently, we reject the hypothesis that *Diplodocus* could have fed by bark stripping. Nevertheless, the bark-stripping FE models indicate the upper limits of *Diplodocus* skull performance, which is of value given the much lower stresses encountered during biting and branch stripping.

In all simulations, localised peaks of high stress are observed in the lateral plates immediately adjacent to the premaxillary teeth (electronic supplementary material, Fig. S1B). The lateral plate is a thin lamina of bone that extends from the main bodies of the dentigerous portions of the tooth-bearing bones to partially cover the bases of functional tooth crowns (Upchurch 1995). Our results support the hypothesis that these structures assist in dissipating feeding-induced stresses that are acting on the bases of the teeth (Upchurch and Barrett 2000). In addition, localised peaks of high stress are absent from the synovial joints, supporting the hypothesis that *Diplodocus* had a functionally akinetic skull (Upchurch and Barrett 2000; Holliday and Witmer 2008).

High stresses occur at the tooth bases, suggesting that these areas may have been vulnerable to mechanical failure, irrespective of the feeding behaviour adopted. Interestingly, diplodocoid sauropods had the highest tooth replacement rates of any vertebrates; in *Nigersaurus*, new teeth erupted every 30 days, whereas in sauropods with broad crowned teeth (e.g. *Camarasaurus*), the replacement rate has been estimated as 62 days (Sereno et al. 2007). It has been suggested that the narrow crowned tooth morphology of diplodocoids, which allows close packing of the teeth within the jaws, evolved in concert with this increase in tooth replacement rates, and that these features were correlated with high rates of tooth wear generated during browsing close to ground level (Chure et al. 2010). However, it is equally plausible that high tooth replacement rates were correlated with a need to regularly replace teeth that were subjected to high stresses, either as a result of static biting or branch stripping, and that might have suffered consequent high rates of tooth loss. Neither of these hypotheses is mutually exclusive.

Diplodocus is not the first extinct taxon with a skull seemingly over engineered for muscle-driven biting. The FE analysis of the contemporaneous theropod dinosaur *Allosaurus* obtained a similar result (Rayfield et al. 2001). While the skull must be able to accommodate a variety of different functions (making it unlikely to be optimised exclusively for feeding), it is unusual that the skull is so resistant to feeding stresses. However, it should be noted that the analyses modelled herein are static, and the cervicocranial musculature would have either retracted or stabilised the head during feeding. The results of our analyses lead us to postulate that the unusual craniofacial form of *Diplodocus* was plausibly an adaptation for certain behavioural strategies associated with food procurement (e.g. branch stripping) and not simply a response to resisting the bite forces produced during jaw closure.

Acknowledgments We thank Clint Davies-Taylor and Neil Gostling for their computing assistance, Karl Niklas and Steven Vogel for their discussion on plant biomechanics, Mike Brett-Surman and Amy Henrici for specimen access, Heather Rockhold for CT scanning and John Whitlock and an anonymous reviewer for their comments on a previous version of this article. We gratefully acknowledge the financial support of the Natural Environment Research Council (NER/S/A/2006/14058) and the Natural History Museum London (awarded to EJR and PMB) and the National Science Foundation (IBN-0407735 to LMW and CMH, and IBN-0343744 and IOB-0517256 to LMW).

References

Bakker RT (1986) The dinosaur heresies. Avon, Bath

Barrett PM, Upchurch P (1994) Feeding mechanisms of *Diplodocus*. Gaia 10:195–203

Calvo JO (1994) Jaw mechanics in sauropod dinosaurs. Gaia 10:183–193

Cattaneo PM, Dalstra M, Melsen B (2005) The finite element method: a tool to study orthodontic tooth movement. J Dent Res 84:428–433

Christiansen P (2000) Feeding mechanisms of the sauropod dinosaurs *Brachiosaurus*, *Camarasaurus*, *Diplodocus*, and *Dicraeosaurus*. Hist Bio 14:137–152

Chure D, Britt BB, Whitlock JA, Wilson JA (2010) First complete sauropod dinosaur skull from the Cretaceous of the Americas and the evolution of sauropod dentition. Naturwissenschaften 97:379–391

Coombs WP Jr (1975) Sauropod habits and habitats. Palaeogeog, Palaeoclimatol, Palaeoecol 17:1–33

Curry KA (1999) Ontogenetic histology of *Apatosaurus* (Dinosauria: Sauropoda): new insights on growth rates and longevity. J Vertebr Paleontol 19:654–665

Dumont E, Piccirillo J, Grosse I (2005) Finite-element analysis of biting behavior and bone stress in the facial skeletons of bats. Anat Rec 283:319–330

Gröning F, Fagan MJ, O'Higgins P (2011) The effects of the periodontal ligament on mandibular stiffness: a study combining finite element analysis and geometric morphometrics. J Biomech 44:1304–1312

Holland WJ (1906) The osteology of *Diplodocus* Marsh. Mem Carnegie Mus 2:225–278

Holland WJ (1910) A review of some recent criticisms of the restorations of sauropod dinosaurs existing in the museums of the United States, with special reference to that of *Diplodocus carnegiei* in the Carnegie Museum. Am Nat 44:259–283

Holland WJ (1924) The skull of *Diplodocus*. Mem Carnegie Mus 9:379–403

Holliday CM (2009) New insights into dinosaur jaw muscle anatomy. Anat Rec A 292:1246–1265

Holliday CM, Witmer LM (2008) Cranial kinesis in dinosaurs: intracranial joints, protractor muscles, and their significance for cranial evolution and function in diapsids. J Vertebr Paleontol 28:1073–1088

Mannion PD, Upchurch P, Carrano MT, Barrett PM (2011) Testing the effect of the rock record on diversity: a multidisciplinary approach to elucidating the generic richness of sauropodomorph dinosaurs through time. Biol Rev 86:157–181

Nalla RK, Kinney JH, Ritchie RO (2003) Mechanistic failure criteria for the failure of human cortical bone. Nat Mater 2:164–168

Niklas KJ (1992) Plant biomechanics. University of Chicago, Chicago

Panagiotopoulou O, Kupczik K, Cobb SN (2011) The mechanical function of the periodontal ligament in the macaque mandible: a validation and sensitivity study using finite element analysis. J Anat 218:75–86

Rayfield EJ (2007) Finite element analysis and understanding the biomechanics and evolution of living and fossil organisms. Annu Rev Earth Planet Sci 35:541–576

Rayfield EJ, Norman DB, Horner CC, Horner JR, Smith PM, Thomason JJ, Upchurch P (2001) Cranial design and function in a large theropod dinosaur. Nature 409:1033–1037

Richmond B, Wright B, Grosse I, Dechow P, Ross C, Spencer M, Strait D (2005) Finite element analysis in functional morphology. Anat Rec A 283:259–274

Sereno PC, Wilson JA, Witmer LM, Whitlock JA, Maga A, Ide O, Rowe TA (2007) Structural extremes in a Cretaceous dinosaur. PLoS One 2:e1230

Toms SR, Eberhardt AW (2003) A nonlinear finite element analysis of the periodontal ligament under orthodontic tooth loading. Am J Orthod Dentofac Orthop 123:657–665

Tornier G (1911) Bau und Lebensweise des *Diplodokus* [sic]. Bericht der Senckenbergischen Naturforschenden Gesellschaft 42:112–114

Upchurch P (1995) The evolutionary history of sauropod dinosaurs. Phil Trans R Soc Lond B 349:365–390

Upchurch P, Barrett PM (2000) The evolution of sauropod feeding mechanisms. In: Sues H-D (ed) Evolution of herbivory in terrestrial vertebrates: perspectives from the fossil record. Cambridge University, Cambridge, pp 79–122

Upchurch P, Barrett PM, Dodson P (2004) Sauropoda. In: Weishampel DB, Dodson P, Osmólska H (eds) The dinosauria, 2nd edn. University of California, Berkeley, pp 259–322

Whitlock JA (2011) Inferences of diplodocoid (Sauropoda: Dinosauria) feeding behavior from snout shape and microwear analysis. PLoS One 6:e18304

Wilson JA, Sereno PC (1998) Early evolution and higher-level phylogeny of sauropod dinosaurs. Soc Vertebr Paleontol Mem 5:1–68

Witzel U, Mannhardt J, Goessling R, De Micheli P, Preuschoft H (2011) Finite element analyses and virtual syntheses of biological structures and their application to sauropod skulls. In: Klein N, Remes K, Gee CT, Sander PM (eds) Biology of the sauropod dinosaurs: understanding the life of giants. Indiana University, Bloomington, pp 171–181

ONLINE SUPPLEMENTARY MATERIAL FOR:

Cranial biomechanics of *Diplodocus* (Dinosauria, Sauropoda): testing hypotheses of feeding behaviour in an extinct megaherbivore

Mark T. Young[1,2§], Emily J. Rayfield[1], Casey M. Holliday[3], Lawrence M. Witmer[4], David J. Button[1], Paul Upchurch[5] and Paul M. Barrett[2,*]

[1] School of Earth Sciences, University of Bristol, Bristol, BS8 1RJ, UK

[2] Department of Palaeontology, The Natural History Museum, London, SW7 5BD, UK

[3] Department of Pathology and Anatomical Sciences, University of Missouri, Columbia, MO 65212, USA

[4] Department of Biomedical Sciences, Ohio University, Athens, OH 45701, USA

[5] Department of Earth Sciences, University College London, London, WC1E 6BT, UK

*Author for correspondence (P.Barrett@nhm.ac.uk)

1) Digital skull reconstruction

The three-dimensional model of a complete *Diplodocus longus* skull (Carnegie Museum of Natural History [CM] in Pittsburgh, PA - CM 11161; figure S1) was created using computed tomography scanning. The skull was scanned at the O'Bleness Memorial Hospital (Athens, OH, USA) in 2003 on a General Electric HiSpeed FX/i Helical CT scanner, producing 290 coronal slices, with 512 transaxial slices in both perpendicular planes, separated by 0.2 mm intervals. The fossil bone was digitally extracted from the surrounding rock matrix using the three-dimensional imaging software AMIRA (v. 4.1.2 Mercury Computing Systems, USA; figure S2A). It was necessary to digitally correct some bones in AMIRA due to breakage, distortion and other imperfections of the fossil. The vomer of CM 11161 had to be reconstructed; breakages in the palatines, jugals, maxillae, and quadratojugals were corrected; and the distortions to the ectopterygoid maxillary processes were corrected. In addition, a hole in the top of the braincase was closed (in the parietal). Witmer et al. (2008) doubted that this hole is in fact the parietal fontanelle in *Diplodocus*. With the exception of the vomer (which is a small bone exposed on the roof of the adductor chamber), no bones had to be reconstructed. Furthermore, no bones were retro-deformed. Once a 3D model was generated it was compared to cranial material held in the Carnegie Museum and the National Museum of Natural History (Washington, D.C.) to aid reconstruction and improve accuracy.

Once satisfied that the AMIRA 3D model was as accurate as possible, segmented slice data were imported into SCANIP v. 2.1 Build 149 (Simpleware Ltd, UK). This software produced a smoothed skull surface model. This three-dimensional surface model was then imported into SCANFE v. 2.0 (Simpleware Ltd, UK). In SCANFE the model was meshed using a voxellated approach, creating a solid geometry consisting of approximately 91% tetrahedral and 9% hexahedral elements. The final volumetric mesh had 906, 257 elements. This mesh was then imported into the FE-software ABAQUS (v. 6.7 Simulia, USA) (figure S2B).

Figure S1. Skull used to create the *Diplodocus longus* skull FE-model. A) lateral view of CM 11161, and B) a close-up on the premaxillary dentition, note the unusual oblique wear facets on the labial surface.

Figure S2. Creation of the *Diplodocus longus* skull FE-model. A) three-dimensional model created from the CT scan slices in the imaging software AMIRA and B) the final three-dimensional FE-mesh in the FE-software ABAQUS.

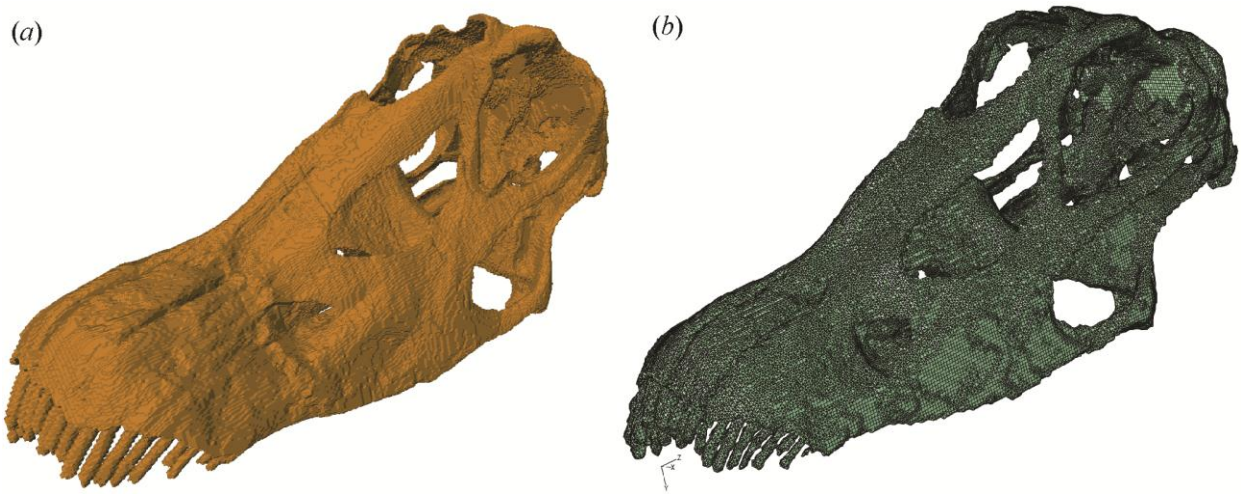

2) Model assumptions (material properties, boundary conditions and loading regime)

Material properties

Material properties and boundary conditions were assigned to the mesh using the FE-software ABAQUS (v. 6.7 Simulia, USA). Although the exact material properties cannot be modelled with true accuracy (Richmond et al., 2005), FE-studies on extinct taxa are also hindered by the inability to directly measure material properties from fossil bone (Rayfield, 2007). As adult Late Jurassic neosauropods (such as *Diplodocus*) are characterised by Haversian bone (Curry, 1999), material properties of extant histological analogues were used as a proxy. Three tissue types were modelled: cranial bone, dentine and enamel, all of which were treated as homogenous and isotropic materials. Although cranial bone is known to be anisotropic (e.g., Zapata et al., 2010), whereas enamel can be isotropic or anisotropic (e.g., see Spears et al., 1993), there is currently no quantitative method to reliably assign anisotropic material properties to long extinct taxa. The method (i.e., see Wroe et al. 2007) for creating heterogeneous models with multiple material properties using CT density values could not be used. This is because CM 11161 has mineralised deposits, such as calcite, that alter the X-ray attenuation data along the CT slice series. Nevertheless, patterns of strain in anisotropic and isotropic FE models are comparable (e.g. Strait et al., 2005), so isotropic models do allow some useful inferences to be made between comparable models or, in the case of this analysis, different loading scenarios applied to the same model. The material properties of tissues in the cranium are poorly known in birds, which constitute one branch of the extant phylogenetic bracket of sauropod dinosaurs (crocodylians and birds). Cranial material property data is known for alligator (Zapata et al., 2010), but following convention we apply material property data based on bovine Haversian bone, which, found in fast growing taxa, may be more appropriate for sauropod dinosaurs. Poisson's ratio value was based upon the transverse axis rather than the longitudinal axis of vertebrate long bones (Reilly & Burstein, 1975). The lowest value (0.29) was taken so not to overestimate cranial strength. A Young's modulus of 23.1 GPa (gigapascals) was based upon Haversian bone in bovine femora (Reilly & Burstein, 1975). The material properties applied to dentine were: Young's modulus =

21 GPa and Poisson's ratio = 0.31 (Gilmore et al., 1969), while for enamel: Young's modulus = 80 GPa and Poisson's ratio = 0.3 (Ichim et al., 2007).

Model constraints

The boundary conditions were also assigned to the mesh using the FE-software ABAQUS (v. 6.7 Simulia, USA). Again, the exact constraints cannot be modelled with true accuracy (Richmond *et al*., 2005); especially as *Diplodocus longus* is a fossil taxon with no extant analogue and has an extreme craniofacial phenotype. To ensure the constraints were as biologically realistic as possible, a distributing coupling constraint (DCC) was applied (in ABAQUS v. 6.7). This type of constraint was chosen as it minimises artificially high stresses in a region that is directly constrained from movement, thus producing a more realistic distribution of cranial stress. The DCC was applied to both the teeth and the jaw joints (figure S3).

Figure S3. Finite-element model of the *Diplodocus longus* skull showing the distributing coupling constraints on: a) jaw joints and b) the premaxillary teeth, in ABAQUS.

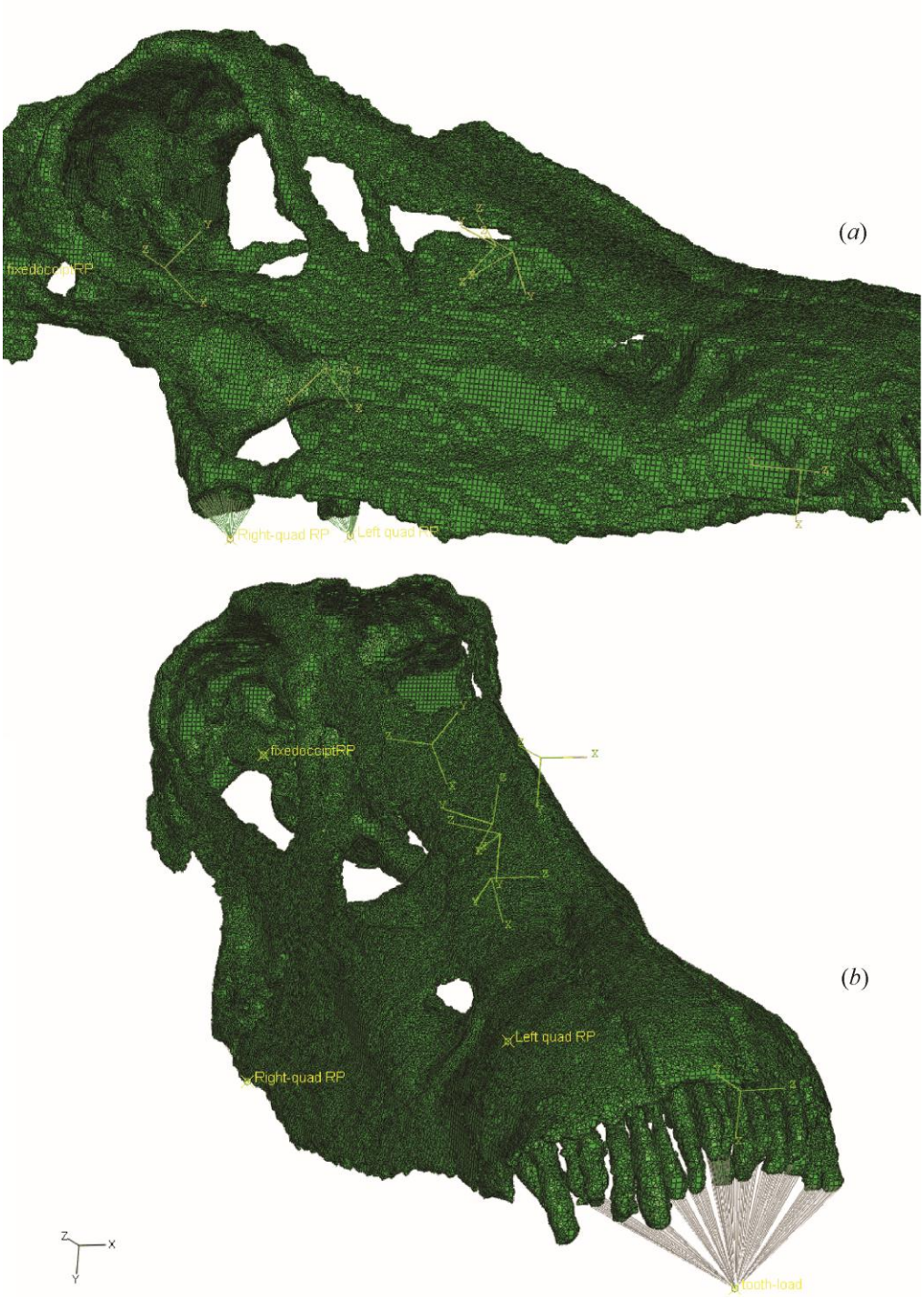

Figure S4. Orientations of forces applied to the skull during static-biting and bark-stripping. Tooth loads are applied parallel to the tooth long axes. Directions of muscle form show by small arrows.

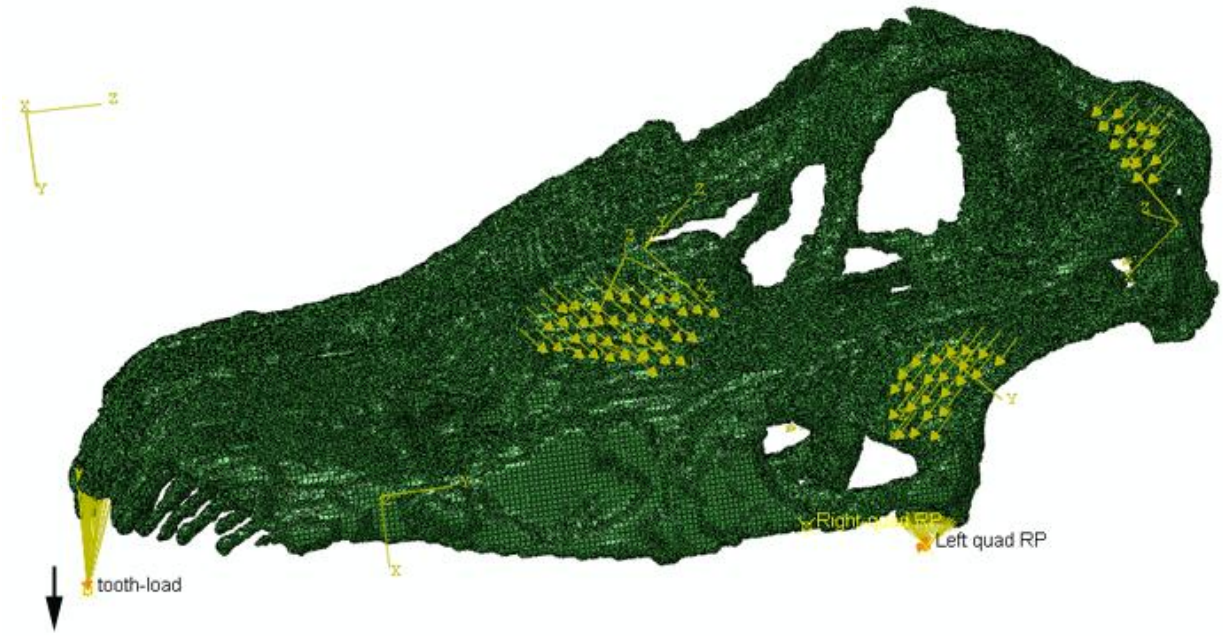

Figure S5. Orientations of forces applied to the skull during branch-stripping. Tooth loads are applied perpendicular to the tooth long axes. Directions of muscle form show by small arrows.

Muscle reconstruction and force generation

Figure S6. Major features of the adductor chamber of *Diplodocus longus* in left lateral aspect. Image is a composite based on CT data (of CM 11161) for skeletal anatomy, while the reconstructed soft-tissue anatomy is based upon osteological correlates. A) superficial dissection, B) adductor chamber musculature origination and insertion sites at superficial depth, C) intermediate depth, D) adductor chamber musculature origination and insertion sites at intermediate depth. Abbreviations: *M. adductor mandibulae externus superficialis*, mAMES; *M. adductor mandibulae externus profundus*, mAMEP; *M. adductor mandibulae posterior*, mAMP; *M. depressor mandibulae*, mDM; *M. pterygoideus dorsalis*, mPTd; *M. protractor pterygoideus*, mPPT; *M. pterygoideus ventralis*, mPTv; *M. pseudotemporalis superficialis*, mPSTs.

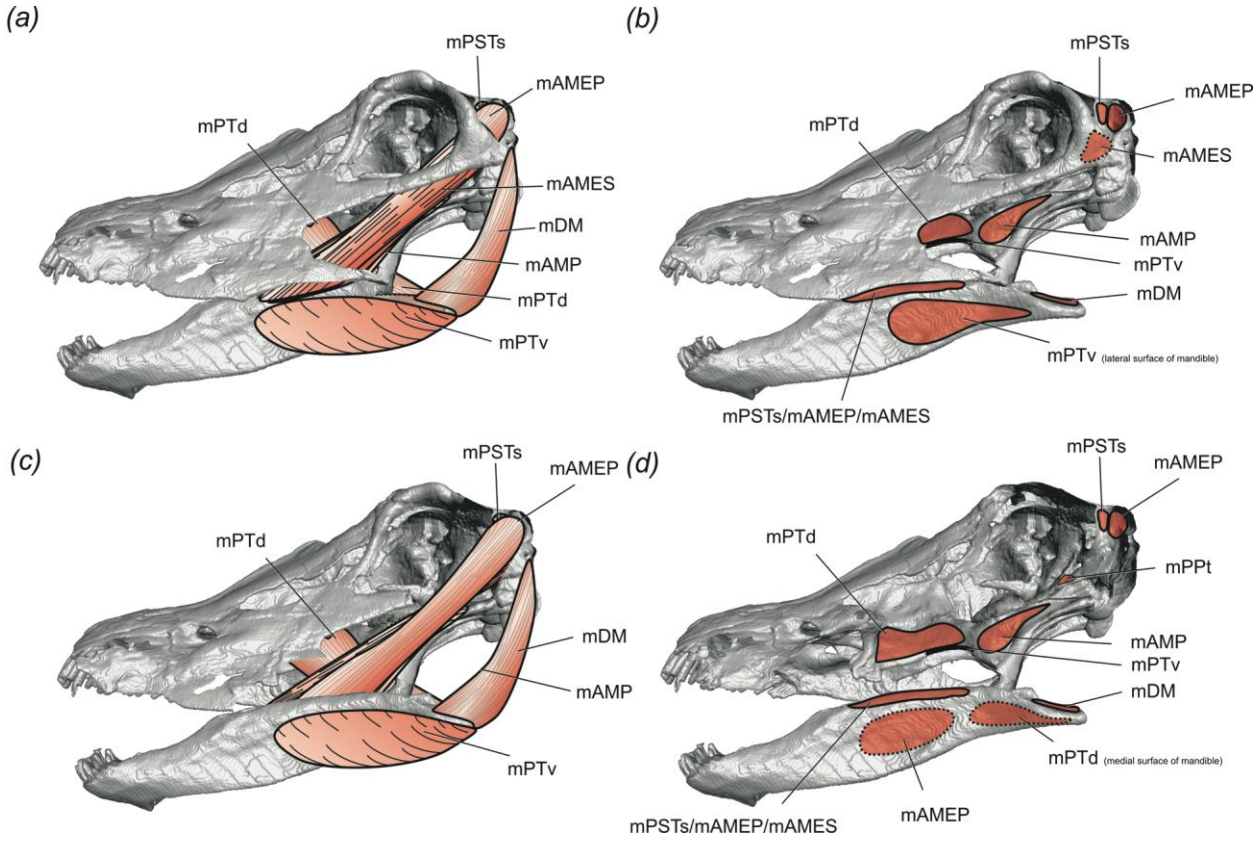

Reconstruction of six adductor muscles (figure S6) follows the methodology of Holliday (2009). The muscle attachment sites were mapped onto the 3D cranial surface model so that their surface areas could be calculated (using STRAND7 FE-software). The volume of each muscle was calculated assuming its shape was a frustum. The muscle attachment sites served as the ends of the frustum, with its length determined to be the maximum distance between the two attachment sites.

$$\text{Frustum Volume} = L/3\,(A_1 + (\text{square-root}[A_1A_2]) + A_2) \qquad \text{Eq. 1}$$

Where L = length of the frustum, A_1 = area of the muscle origination site, A_2 = area of the muscle insertion site.

The calculated muscle volume was used to estimate physiological cross-sectional area by using the maximum length of the muscle as the base fibre length. While it is unlikely this method will give the true fibre length, due to the adductor musculature having at least a small degree of pinnation, to minimise *ad hoc* assumptions the muscles were modelled without pinnation. Although the muscle contractile forces are equal to maximal cross-sectional area multiplied by specific tension (Wroe et al., 2005), one cannot determine the exact specific tension for fossil taxa. Here the physiological cross-sectional area was multiplied by the maximum known specific tension of vertebrate adductor muscles (392 kPa; see Thomason et al., 1990). These muscle forces assume 100% contraction (muscle force magnitudes are listed in Table S1). The muscle contractile forces were applied directly to the nodes of the FE-mesh and oriented in the line of action suggested by the reconstruction.

Calculated muscle forces (Table S1)

Muscle contractile forces				muscle volume (m^3)	PCSA (m^2)	Muscle force N	Muscle force N
	Cranial attachment area (m^2)	Mandibular attachment area (m^2)	approximate length between attachments (m)	volume of a frustrum	muscle volume / fibre length	PCSA x specific tension lower (147 kPa)	PCSA x specific tension upper (392 kPa)
mAMEP	1.30E-03	7.88E-04	0.256	2.65E-04	1.03E-03	152	405
mPSTs	9.06E-04	4.23E-04	0.2505	1.62E-04	6.48E-04	95	254
mAMP	3.22E-03	3.41E-03	0.0952	3.15E-04	3.31E-03	487	1299
mPTd	4.29E-03	2.69E-03	0.157	5.43E-04	3.46E-03	508	1355
mPTv	3.55E-04	3.20E-03	0.134	2.06E-04	1.54E-03	226	603
mAMES	1.06E-03	2.28E-03	0.1751	2.86E-04	1.63E-03	240	640

Abbreviations as before.

Calculated branch and bark stripping forces (Table S2)

	Branch-stripping	Bark-stripping
Yield Stress (Nm^{-2})	1.00E+06	7.30E+06
Area of tooth-contact (m^2)	2.50E-05	2.50E-05
	Newtons	Newtons
4 teeth	100	730
8 teeth	200	1460
14 teeth	350	2555

Reaction forces (N) at the craniomandibular joint (Table S3)

Model	Static bite	Branch-stripping	Bark-stripping
4 teeth	3147.02	3146.94	3168.39
8 teeth	3147.01	3147.82	3239.43
14 teeth	3147.00	3150.89	3431.79

3) Additional images of the three *Diplodocus* feeding models

Figure S7. *Diplodocus longus* skull von Mises stress contour plots for the static biting model, in: A) lateral view, B) dorsal view, C) ventral view and D) frontal view.

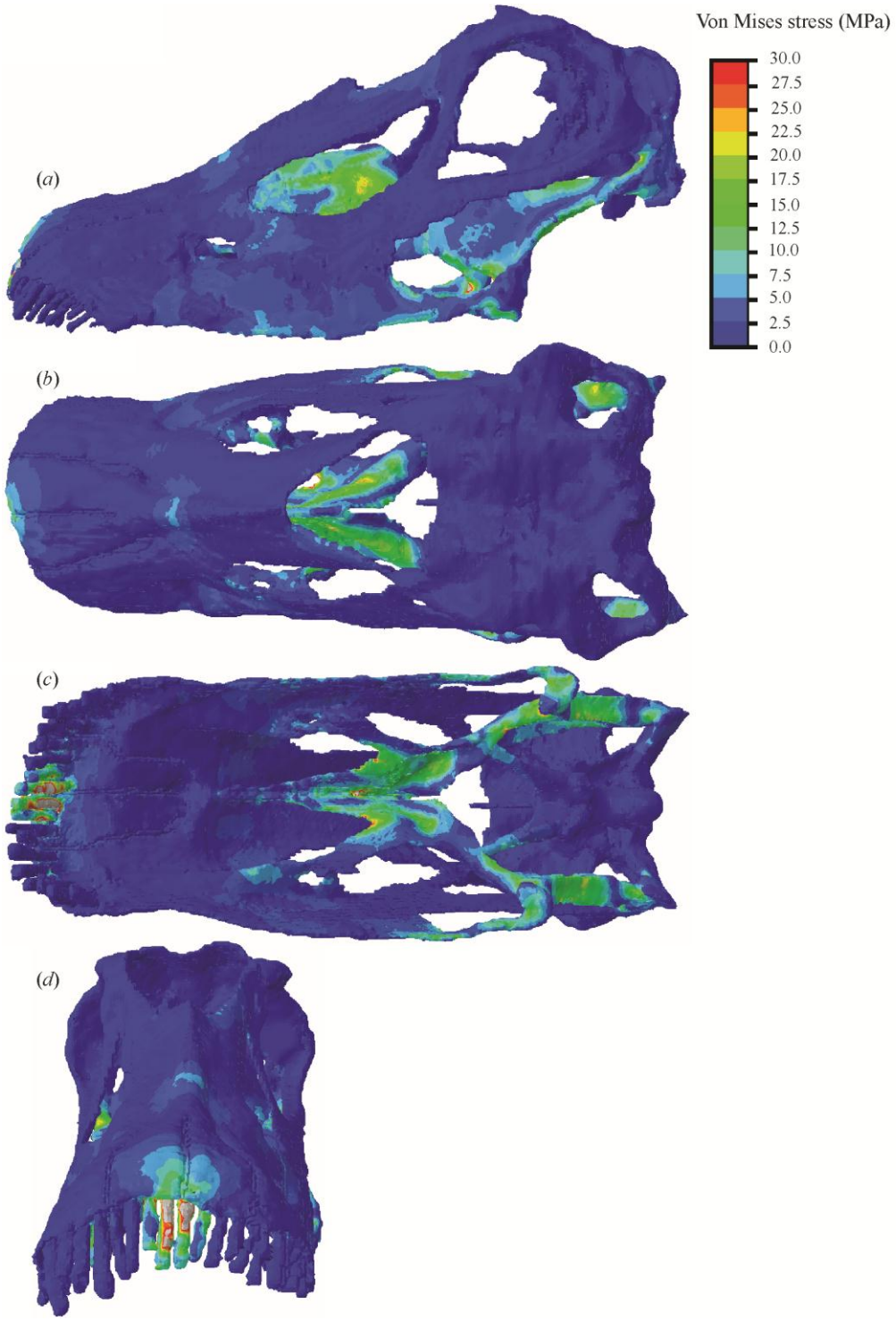

Figure S8. ***Diplodocus longus*** **skull von Mises stress contour plots for the branch stripping model, in: A) lateral view, B) dorsal view, C) ventral view and D) frontal view.**

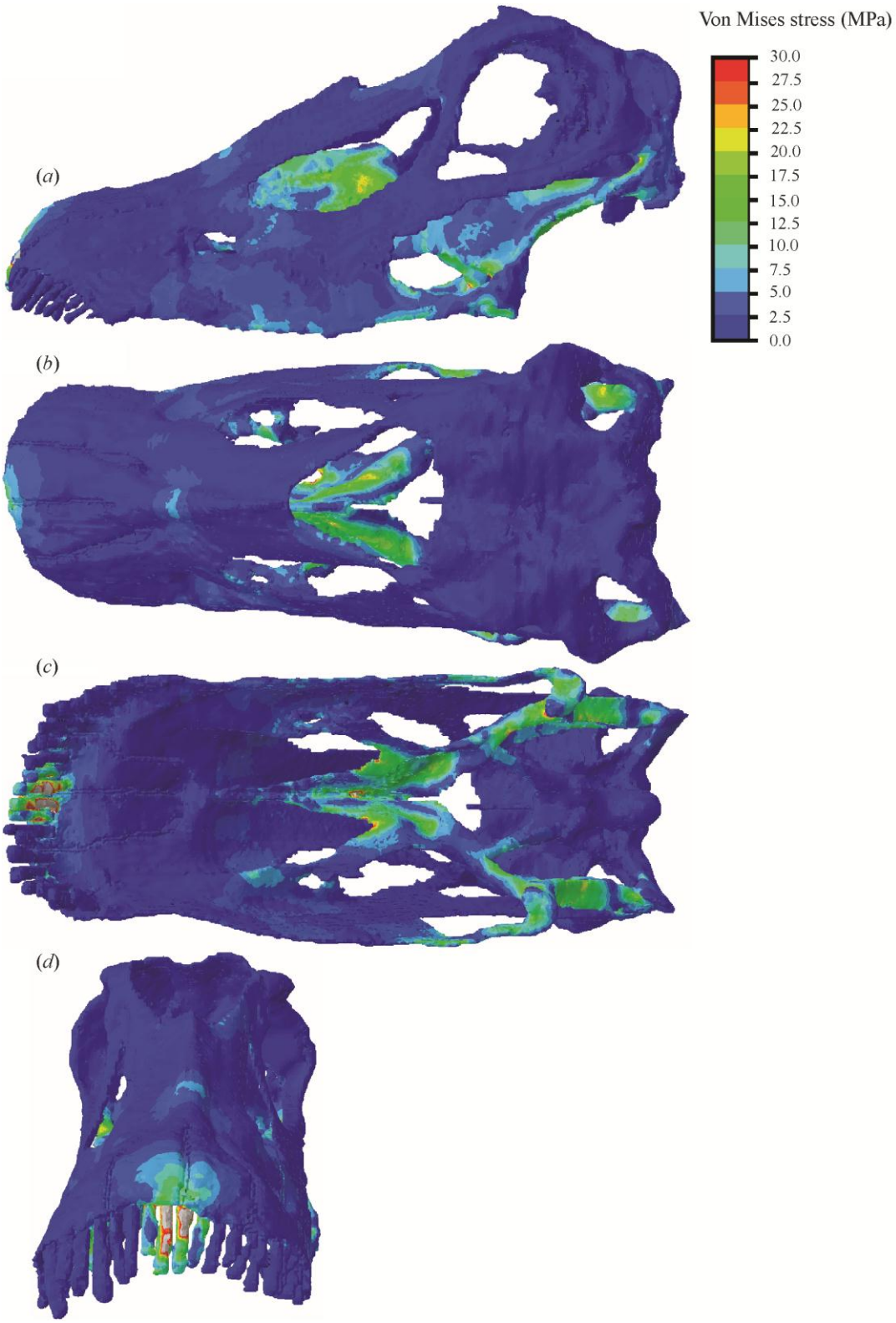

Figure S9. ***Diplodocus longus*** **skull von Mises stress contour plots for the bark stripping model, in: A) lateral view, B) dorsal view, C) ventral view and D) frontal view.**

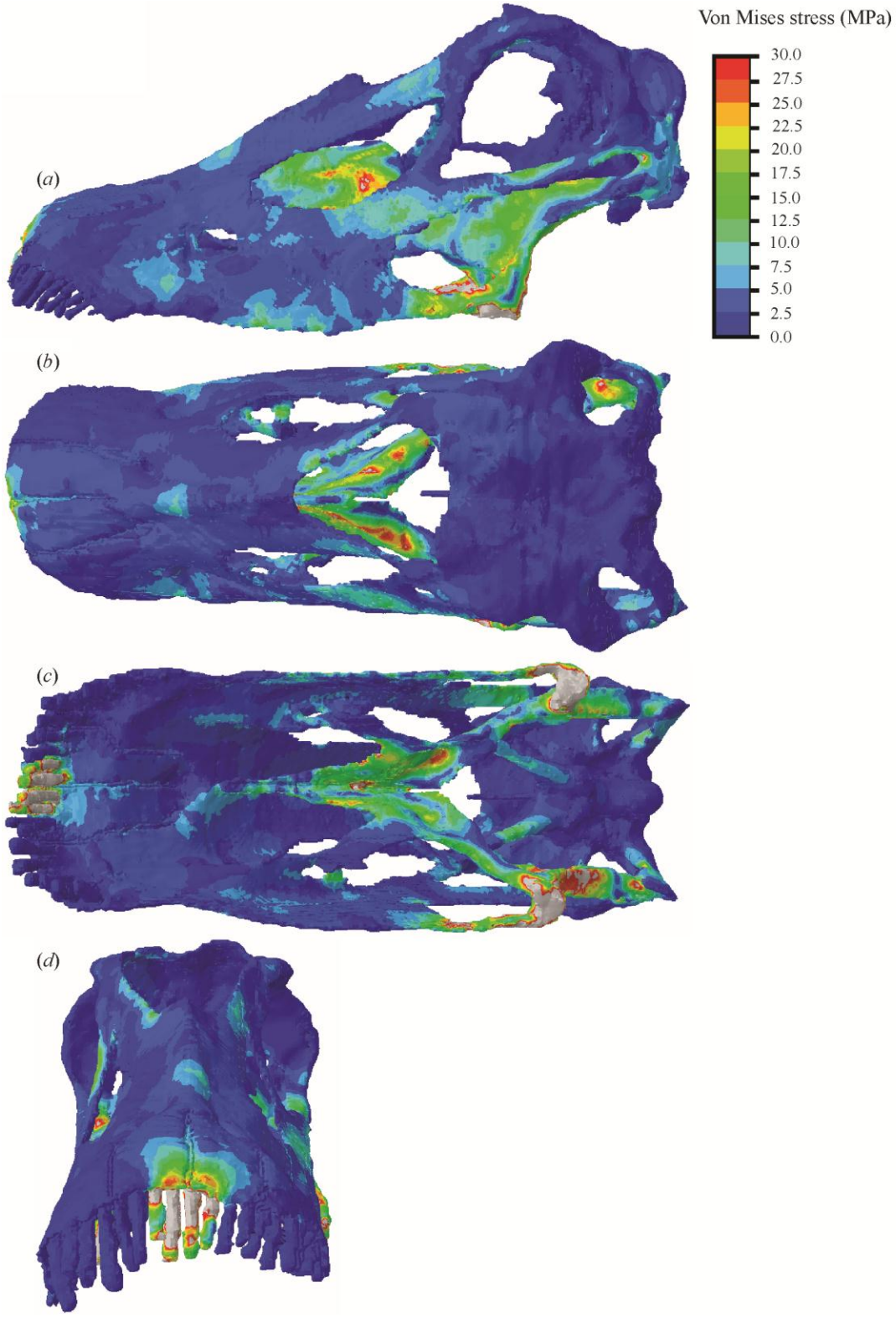

4) Exact locations of the 16 nodal loci

Locations of the 16 nodal loci used in Figure 2 (Table S4)

Locus number	Anatomical location
1	suture between postorbital and squamosal within the infratemporal fenestra
2	midpoint along the dorsal margin of the quadratojugal, within the infratemporal fenestra
3	suture between maxilla and lacrimal within the antorbital fenestra
4	suture between premaxilla and maxilla within the external nares
5	suture between ectopterygoid and maxilla (ventral surface)
6	midpoint along the palatine midline (ventral surface)
7	suture between basipterygoid process and pterygoid (ventrocaudal surface)
8	suture between paroccipital process and quadrate (dorsocaudal surface)
9	inflexion point of the quadratojugal along the ventral margin
10	maxilla external surface immediately ventral to the preantorbital fenestra
11	premaxilla-premaxilla suture along the midline, at the point immediately caudal to where the dentigerous regions converge to form the ascending processes (external surface)
12	external surface of the parietal, at the midpoint along the midline
13	suture between maxilla and quadratojugal (lateral face of the skull, external surface)
14	midpoint of the quadratojugal beneath the infratemporal fenestra (lateral face of the skull, external surface)
15	premaxilla-premaxilla suture along midline of the dentigerous region (external surface)
16	distal region of the medial-most left premaxillary tooth (rostral surface)

5) Sensitivity analyses

After our initial results, we subsequently tested how sensitive the results are to: 1) the number of teeth constrained/loaded and 2) the fact that we used the highest possible specific tension for the adductor muscles. In both tests the same FE-mesh was used, with the same methodology as before, but with specific differences.

The first sensitivity test involved two further iterations of the FE-analysis, altering the DCC to constrain not four teeth but, a) the 8 mesial-most teeth and b) the 14 mesial-most teeth. In addition, for the branch-stripping and bark-stripping models we also altered the loading regime to account for the additional teeth constrained (see Table S2). This resulted in six new FE-contour plots (static biting with 8 teeth constrained, static biting with 14 teeth constrained, branch-stripping with 8 teeth loaded and constrained, branch-stripping with 14 teeth loaded and constrained, bark-stripping with 8 teeth loaded and constrained, and bark-stripping with 14 teeth loaded and constrained).

These six new simulations, and the original three, are shown in figure S10. As can be seen, there is very little difference between the three static-biting simulations (figure S10A-C). All that is

altered is the stress distribution in the constrained teeth and the adjacent dentigerous bone, i.e. when more teeth are constrained peak stress in the dentigerous region of the premaxilla lowers and becomes more widely distributed across the front of the snout, similarly the stress in the teeth decreases. This pattern is replicated in the four new stripping action models (figure S10E-F, H-I). These models all exhibit another pattern, a generalised increase in stress in the thinner regions of the skull (lateral portions of the maxillae and the ascending processes, quadratojugals, and jugals). In the branch-stripping models, the stress increase in these more fragile areas of the skull is negligible (figure S10D-F). However, in the bark-stripping models there is a more pronounced increase in cranial stress, particularly in these fragile areas (figure S10G-I). Interestingly, when 14 teeth are loaded and constrained for the bark-stripping model the entire premaxilla is stressed, as is the entire dentigerous region of both the premaxilla and maxilla, anterolateral margins of the external nares, and peaks of high stress accumulating at points along the skull ventral margin and the lower temporal bar (figure S10I). These additional simulations help to re-enforce how unlikely bark-stripping is as a potential feeding behaviour, and how even dramatically increasing the number of teeth being loaded does not make branch-stripping any less likely.

In the second test we reduced the specific tension of the adductor muscles (to 147 kP). The resultant change in adductor muscle forces that were applied to the models are in Table S1. All other variables were kept constant. As one would expect, the overall stress magnitudes are lower for all three models, but the patterns are the same. This is to be expected as the different muscle forces, although decreased in magnitude, are still proportionally the same.

Figure S10. ***Diplodocus longus*** **skull von Mises stress contour plots for the sensitivity analysis (tooth count variation). Contour plots A-C are the static-biting model, contour plots D-F are the branch-stripping model, and contour plots G-I are the bark stripping models. Contour plots (A), (D) and (G) have the 4 medial most teeth fixed (i.e., the default within this paper). Contour plots (B), (E) and (H) have the 8 medial most teeth fixed. Contour plots (C), (F) and (I) have the 14 medial most teeth fixed.**

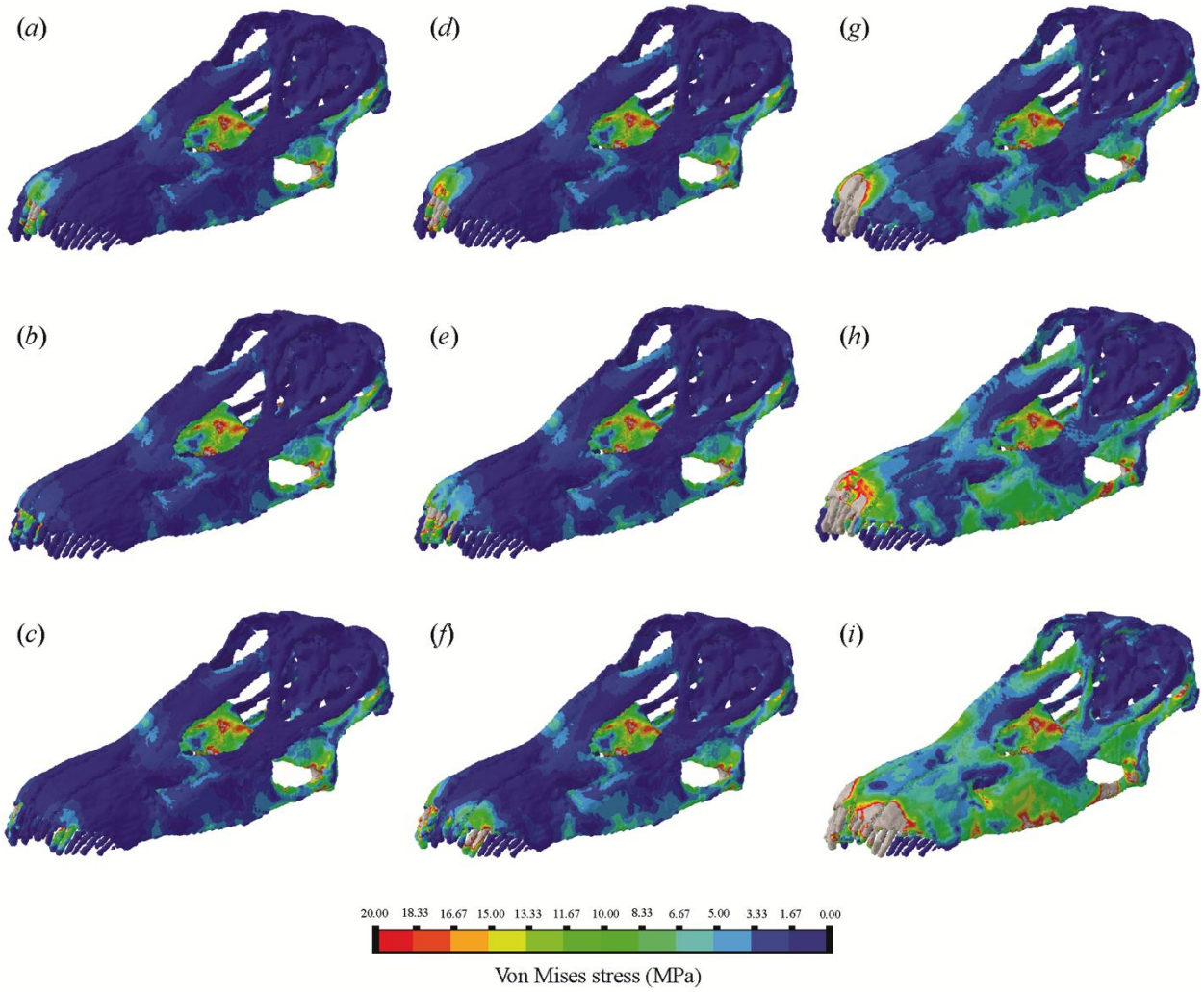

6) Supplementary references

References cited in this online supplement can be found either in the bibliography of the main article or, when not cited in the latter, in the supplementary reference list below.

Gilmore RS, Pollack RP, Katz JL (1969) Elastic properties of bovine dentine and enamel. Arch Oral Biol 15:787–796.

Ichim I, Schmidlin PR, Kieser JA, Swain MV (2007) Mechanical evaluation of cervical glass-ionomer restorations: 3D finite element study. J Dent 35:28–35.

Reilly D, Burstein A (1975) The elastic and ultimate properties of compact bone tissue. J Biomech 8:393–405.

Spears IR, van Noort R, Crompton RH, Cardew GE (1993) The effects of enamel anisotropy on the distribution of stress in a tooth. J Dent Res **72**:1526–1531.

Strait DS, Wang Q, Dechow PC, Ross CF, Richmond BG, Spencer MA, Patel BA (2005) Modeling elastic properties in finite element analysis: how much precision is needed to produce an accurate model? Anat Rec A 283:275–287.

Thomason JJ, Russell AP, Morgeli M (1990) Forces of biting, body size, and masticatory muscle tension in the opossum *Didelphis virginiana*. Can J Zool 68:318–324.

Witmer LM, Ridgely RC, Dufeau DL, Semones M C (2008) Using CT to peer into the past: 3D visualization of the brain and ear regions of birds, crocodiles, and nonavian dinosaurs. In: Endo, H., Frey, R. (eds.) Anatomical Imaging: Towards a New Morphology. Springer-Verlag, pp. 67–88.

Wroe S, Clausen P, McHenry C, Moreno K, Thomason J. (2005) Computer simulation of feeding behavior in the thylacine and dingo as a novel test for convergence and niche overlap. Proc R Soc Lond B 274:2819–2828.

Wroe S, McHenry C, Thomason J (2005) Bite club: comparative bite force in big biting mammals and the prediction of predatory behaviour in fossil taxa. Proc R Soc Lond B 272:619–625.

Zapata U, Metzger K, Wang Q, Elsey RM, Ross C, Dechow PC (2010) Material properties of mandibular cortical bone in the American alligator, *Alligator mississippiensis*. Bone 46:860–867.